NANO LETTERS

Letter

pubs.acs.org/NanoLett

Multifactorial Modulation of Binding and Dissociation Kinetics on Two-Dimensional DNA Nanostructures

Alexander Johnson-Buck,[†] Jeanette Nangreave,[‡,§] Shuoxing Jiang,[‡,§] Hao Yan,[‡,§] and Nils G. Walter*[,†]

[†]Department of Chemistry, Single Molecule Analysis Group, 930 N. University Avenue, University of Michigan, Ann Arbor, Michigan 48109-1055, United States

[‡]The Biodesign Institute, Arizona State University, Tempe, Arizona 85287, United States

[§]Department of Chemistry and Biochemistry, Arizona State University, Tempe, Arizona 85287, United States

Supporting Information

ABSTRACT: We use single-particle fluorescence resonance energy transfer (FRET) to show that organizing oligonucleotide probes into patterned two-dimensional arrays on DNA origami nanopegboards significantly alters the kinetics and thermodynamics of their hybridization with complementary targets in solution. By systematically varying the spacing of probes, we demonstrate that the rate of dissociation of a target is reduced by an order of magnitude in the densest probe arrays. The rate of target binding is reduced less dramatically, but to a greater extent than reported previously for one-dimensional probe arrays. By additionally varying target sequence and buffer composition, we provide evidence for two distinct mechanisms for the markedly slowed dissociation: direct hopping of targets between adjacent sequence-matched probes and nonsequence-specific, salt-bridged, and thus attractive electrostatic interactions with the DNA origami pegboard. This kinetic behavior varies little between individual copies of a given array design and will have significant impact on hybridization measurements and overall performance of DNA nanodevices as well as microarrays.

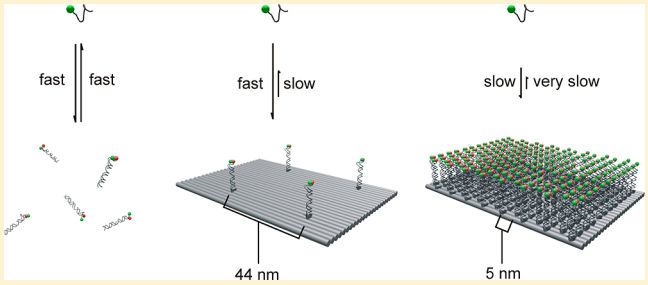

KEYWORDS: *DNA origami, DNA nanotechnology, kinetics, single molecule, single-particle FRET*

In recent years, a number of addressable DNA-origami-based nanopegboards have been designed to capture and organize molecular components by site-specific hybridization.[1−6] Many of these devices are dynamic, with hybridization reactions or conformational changes playing a crucial role in their assembly and function.[1−3,6] In addition, strand displacement reactions can be used to induce global conformational changes or topological reconfigurations in DNA origami, making it possible to rationally control dynamic nanomechanical processes such as the opening of a lid,[7] release of nanoparticle cargo,[8] and reconfiguration of a Möbius strip into two interlocking rings.[9] In the near future, similar devices may be integrated with DNA computing[10] or biological[11] circuits for enhanced control over their timing and operation.[12] For such approaches to be successful, a quantitative understanding of the kinetics and thermodynamics of DNA hybridization to probes on DNA origami is critical.

The kinetics and thermodynamics of DNA hybridization have been extensively characterized in the context of self-assembled monolayers (SAMs) of single-stranded DNA (ssDNA), revealing many differences from the corresponding reactions in bulk solution. For example, it has been reported that higher densities of ssDNA probes in SAMs slow the association kinetics of complementary ssDNA targets[13] and enhance thermodynamic selectivity for perfectly matched over mismatched targets.[14] In addition, the yield of probe-target hybridization was found to be reduced in many ssDNA SAMs with high densities of probes ($>10^{12}$ cm^{-2}).[15−17] This effect is mitigated when the DNA is deposited on the surface via nanografting from an AFM tip, suggesting that disorder within crowded SAMs may be a more important obstacle to hybridization than steric hindrance.[18] Despite this wealth of literature on solid-phase DNA hybridization, there have been only a few studies of hybridization at the surface of DNA nanostructures.[19,20]

The organization of oligonucleotide probes into regular arrays on designed DNA nanopegboards may influence hybridization kinetics in a variety of ways. First, it is likely that the electrostatic environment in the vicinity of a DNA nanostructure differs from that in bulk solution; two- and three-dimensional DNA origami near neutral pH possess a high density of negatively charged phosphates, and their folding is sensitive to metal ion concentration.[21] In general, nucleic acids form both diffuse and site-specific interactions with metal cations, which screen the negative charge of the phosphate

Received: March 15, 2013
Revised: May 14, 2013
Published: May 23, 2013

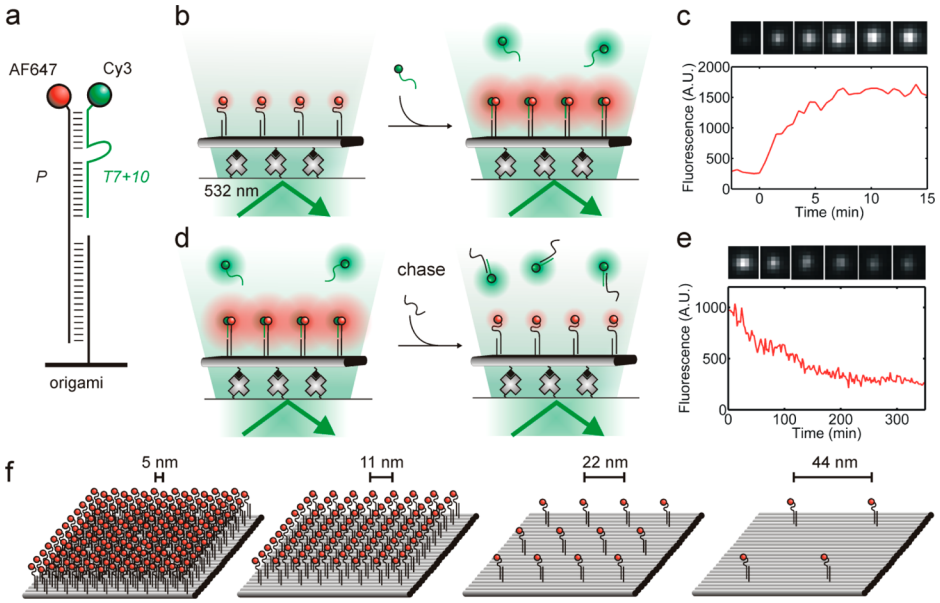

Figure 1. (a) A Cy3-labeled DNA target (*T7+10*; alternatively *T11* or *T11O*) binds to multiple copies of the AF647-labeled probe (*P*) oligonucleotide within an origami-templated array or nanopegboard. (b) Upon addition of 25−100 nM target strand, the binding of the target to the probe is visualized by FRET on a TIRF microscope. (c) The binding of multiple (4−187) copies of the donor-labeled target leads to a gradual increase in the acceptor (AF647) signal on a single DNA origami array. (d, e) Upon removal of excess target and addition of unlabeled *P* as a chase, bound target dissociates from the origami array without a chance to rebind, resulting in a loss of FRET signal from a single DNA origami array. (f) Schematics of the four DNA origami arrays used in this study, each bearing multiple copies of *P* spaced by approximately 5, 11, 22, or 44 nm.

backbone and stabilize more compact conformations, including duplexes.[22−24] Second, the organization of probes into dense arrays may alter hybridization kinetics through steric crowding or physical interactions between adjacent probe sites, as in the case of ssDNA SAMs. Finally, owing to their complex construction, variable assembly yield, and small copy numbers of components, the functional behavior may vary between individual copies of DNA nanodevices,[25,26] and it is important to understand their idiosyncrasies at the single-copy level.

Two previous reports found relatively minor differences between the hybridization behavior in bulk solution and that on DNA nanostructures.[19,20] In one of these studies, the binding of a 20-nucleotide ssDNA target to the complementary sequence at the edge of a 6-helix DNA tile was found to be ∼20−30% slower when the binding site was flanked on two sides by noncomplementary DNA.[20] However, neither of these reports examined the impact of two-dimensional crowding of probes on target binding, a configuration commonly encountered on nanostructures and expected to pose greater steric obstacles to binding, as well as a greater potential for interactions between adjacent sites. Furthermore, the influence of the spacing between probes on hybridization kinetics, including the dissociation of bound targets, has not been examined systematically, nor has the reproducibility of kinetic behavior between individual copies of a DNA nanostructure.

To address these questions, we used fluorescence resonance energy transfer (FRET) to measure the kinetics of hybridization on individual surface-immobilized DNA origami arrays with varying probe densities and compared these to the kinetics in bulk solution. The DNA arrays were immobilized on a microscope slide, which permitted time-lapsed observation of individual arrays and prevented interactions between them. Upon binding of a target labeled with a FRET donor (Cy3) to an oligonucleotide probe (*P*) labeled with a FRET acceptor (Alexa Fluor 647, or AF647), the excited donor transfers energy to the acceptor, which fluoresces (Figure 1a,b). The increase in acceptor signal was detected using total internal reflection fluorescence (TIRF) microscopy, yielding measurements of target binding to dozens of individual DNA arrays in parallel (Figure 1b,c). Furthermore, by adding a chase consisting of excess unlabeled *P* in solution, we monitored the kinetics of target dissociation from an individual probe array through the loss of FRET (Figure 1d,e). The chase was added at a concentration of 500 nM, which is at least a 5-fold excess over the target. Increasing the chase concentration to 5 μM did not alter the apparent rate constant of target dissociation (rate constants were within one standard error of the mean, or SEM, for all targets), suggesting that the chase does not actively displace the target from *P* but merely sequesters a free target as it dissociates. Importantly, although we found AF647 to self-quench at the highest probe densities, leading to a nonlinearly increasing fluorescence signal, the increase in FRET instead was found to depend linearly on probe density within the range of spacings considered (Supporting Figure S1). This feature allowed us to use FRET to directly measure and compare binding and dissociation rate constants at varying probe densities, without correction factors. Furthermore, the steep distance dependence of FRET enabled us to perform corresponding control measurements for probe-target pairs in free solution. While fluorescent labeling can significantly perturb the kinetics of hybridization,[27,28] we assume that any contribution from the labels will be similar for all targets and probe densities since we hold our labeling scheme constant.

We measured kinetics in 1× HBS buffer (50 mM HEPES-KOH, pH 7.2, 150 mM NaCl) at 20 °C for arrays with spacings of ∼5−44 nm between nearest-neighbor probes (corresponding to probe densities of ∼4 × 10^{12} to ∼0.05 × 10^{12} cm^{-2}, respectively; Figure 1f, Supporting Figure S2). We used the 8−17 deoxyribozyme sequence (*T7+10*, Figure 1a, Supporting Figure S3) as a target because of its prior use as a leg for DNA

dx.doi.org/10.1021/nl400976s | *Nano Lett.* 2013, 13, 2754−2759

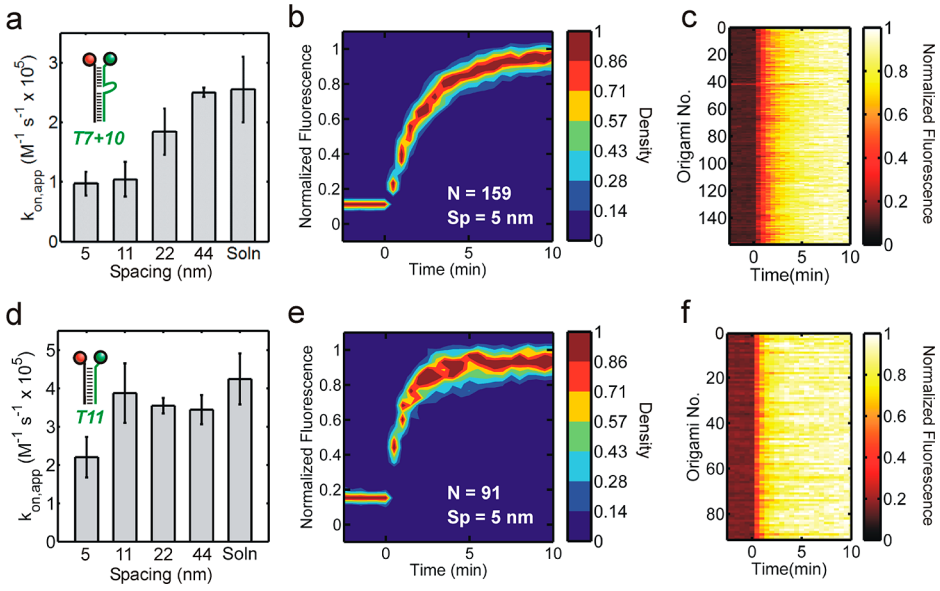

Figure 2. (a) Kinetics of target *T7+10* binding to probe on origami with different spacings (5−44 nm) and in free solution ("Soln"). (b,c) Probability density map (b) and single-origami trajectories (c) of AF647 signal increase upon binding of 75 nM *T7+10* to probe on origami spaced by 5 nm. (d) Kinetics of target *T11* binding to probe on origami and in solution. (e,f) Probability density map (e) and single-origami trajectories (f) of AF647 signal increase upon binding of 75 nM *T11* to probe on origami spaced by 5 nm. Error bars are one SEM.

walkers autonomously moving along probe arrays[1,3] (<2.5% of *P* is cleaved by *T7+10* on the time scale of our measurements due to the lack of a divalent metal ion cofactor; see Supporting Figure S4), as well as for its two independent binding arms, which we reasoned might yield nonstandard kinetic behavior in dense probe arrays. Measuring the kinetics of *T7+10* binding to *P* under pseudo-first-order conditions (with *T7+10* in excess), we found that binding is just as rapid on an origami template with 44 nm probe spacing as in free solution (Figure 2a, Supporting Figure S5), consistent with previous results for isolated probes on DNA nanostructures.[19,20] As the spacing between probes is decreased from 44 to 5 nm, however, binding is slowed approximately 2.5-fold (Figure 2a, Supporting Figure S5). This effect is more pronounced than reported previously in one-dimensional arrays of probes on DNA nanostructures,[20] consistent with the notion that a two-dimensional array provides a more sterically crowded environment. Nonetheless, the relative increase in A647 fluorescence (~5-fold) upon target binding is similar for all probe spacings (Supporting Figure S6), suggesting that neither steric crowding nor nonspecific probe−probe interactions reduce the overall yield of target binding. To determine what contribution *T7+10*'s two separate binding arms make to slowing its binding rate constant, we characterized an additional target, termed *T11*, that possesses similar binding kinetics as *T7+10* but forms only a single 11-base pair helix upon binding to *P* (Figure 2d, Supporting Figure S3). The slowing of *T11* binding occurs only with probe spacings <11 nm, suggesting that this smaller oligonucleotide can more successfully hybridize to probes within a crowded array. However, the relative reduction in the rate constant of *T11* binding in the most crowded array is similar to that for *T7+10*. While the slowing of target association is more pronounced than in one-dimensional arrays, it depends less steeply on target density than reported for SAMs of ssDNA probes at similar density regimes.[29] In fact, our finding that the hybridization yield is independent of probe spacing is consistent with a report that well-ordered, nanografted ssDNA SAMs can yield efficient hybridization even at high densities[18] and further suggests that designed DNA nanopegboards can perform this same organizational role.

We also examined the extent of variability in binding kinetics between individual origami tiles. For both *T11* and *T7+10*, the association reaction approaches deterministic behavior at high target densities due to the large number of targets binding to each array, with little variation between individual origami tiles (Figure 2b,c,e,f). If each origami trajectory is fit individually, the observed pseudo-first-order rate constants for association to arrays with 5-nm spacing as an example are 0.46 ± 0.11 min^{-1} and 0.97 ± 0.24 min^{-1} for 75 nM *T7+10* and *T11*, respectively (error bounds are one standard deviation). Furthermore, kinetic Monte Carlo simulations (Supporting Figure S7) suggest that most or all of the variation between kinetic trajectories of individual origami at the different spacings (Supporting Figure S8) can be attributed to statistical noise (i.e., variation in the exponentially distributed wait times for a single reaction to occur) and noise in the measurement. Accordingly, when the number of probes per array decreases, the experimental reaction trajectories vary to a greater extent between arrays. In separate work, we recently showed that the kinetics of DNA hybridization can vary across the surface of a single DNA nanopegboard in an idiosyncratic manner dependent on target sequence and probe density, most likely due to assembly and topological variations.[26] The narrow distribution of rate constants we find here for the denser arrays further suggests, however, that such variability across an origami tile is averaged out to yield a kinetic performance that is reproducible between individual DNA nanostructures, as long as averaging occurs over a sufficient number of features. This will likely be a useful property for interfacing with molecular computing systems,[10,30−32] especially if the nanostructures are required to function as discrete, autonomous components. We suggest that care should be taken to ensure sufficient copy numbers of elements and appropriate network architectures to afford suitably robust behavior.

Compared to the association reaction, the rate constant of *T7+10* dissociation from origami arrays deviates even more

dx.doi.org/10.1021/nl400976s | *Nano Lett.* 2013, 13, 2754−2759

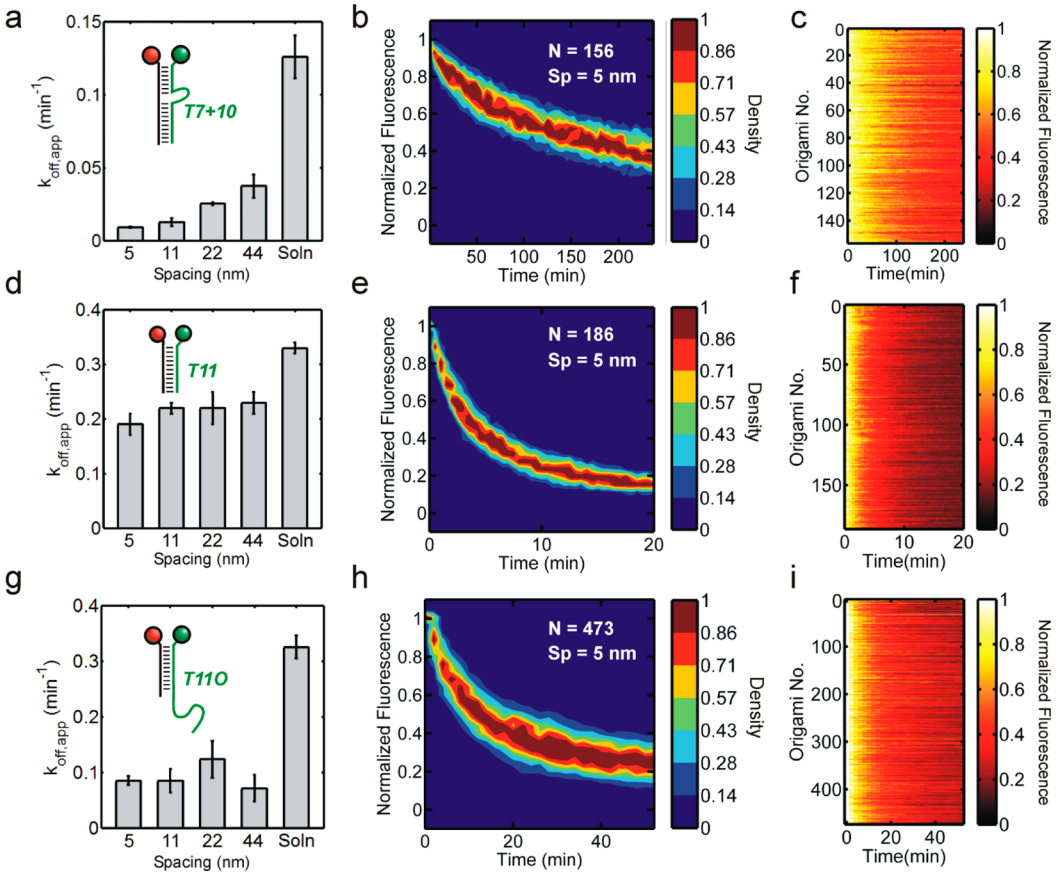

Figure 3. (a) Kinetics of target *T7+10* dissociation from probe on origami with different spacings (5−44 nm) and in free solution ("Soln"). (b,c) Probability density map (b) and single-origami trajectories (c) of AF647 signal decrease upon dissociation of *T7+10* from probe on origami spaced by 5 nm. (d) Kinetics of target *T11* dissociation from probe on origami and in free solution. (e,f) Probability density map (e) and single-origami trajectories (f) of AF647 signal decrease upon dissociation of *T11* from probe on origami spaced by 5 nm. (g) Kinetics of target *T11O* dissociation from probe on origami and in free solution. (h,i) Probability density map (h) and single-origami trajectories (i) of AF647 signal decrease upon dissociation of *T11O* from probe on origami spaced by 5 nm. Error bars are one SEM.

dramatically from the reaction in free solution, decreasing by ∼3.5-fold and ∼10-fold at probe spacings of 44 and 5 nm, respectively, with a clear dependence on spacing (Figure 3a−c). Utilizing the rate constants in Figures 2 and 3, the dissociation equilibrium constant for *T7+10* binding to *P* derives as $K_d = k_{off}/k_{on}$ and is ∼4- to 5-times lower (tighter) at the surface of an origami tile (1.6−2.4 nM) than in free solution (8.2 nM), with slightly smaller K_d values at the closest probe spacings due to their considerably decreased k_{off}. In contrast, the rate constant of *T11* dissociation from origami is only about 35% slower than in solution and shows little or no spacing dependence (Figure 3d−f). Consequently, the resultant K_d values for *T11* dissociation from *P* on an origami array (10.9−14.3 nM) are similar to the value in free solution (13.0 nM). We conclude that, while the thermodynamics of *T11* binding to *P* are affected little in the context of a DNA nanostructure, the dramatically reduced dissociation rate constant of *T7+10* from the nanostructure results in a net stabilization of binding despite the concomitant slight slowing of association.

To investigate whether the differences between *T7+10* and *T11* result from their different size (32 and 11 nucleotides, respectively) or their distinct modes of probe binding (two and one helical domain, respectively), a third target sequence *T11O* was designed with the same 11-nucleotide binding sequence as *T11* but the overall length and base composition of *T7+10*. To accomplish this, we added a 21-nucleotide 3′-overhang of random sequence to the *T11* design (Figure 3g, Supporting Figure S3). Like *T7+10* on the 44-nm-spaced origami array, *T11O* exhibits a rate constant of dissociation from origami-bound *P* that is about 3- to 4-fold slower than in solution; however, like *T11*, this rate constant does not decrease further at smaller probe spacings (Figure 3g−i). We interpret these observations as evidence of at least two mechanisms for the slowing of oligonucleotide dissociation from origami-templated probe arrays: (i) a spacing-dependent walking (or hopping) mechanism observed for *T7+10* with its two binding arms but not the one-arm *T11* or *T11O*; and (ii) a spacing-independent mechanism by which the longer DNA strands *T7+10* and *T11O* are retained more strongly than the shorter *T11*. Notably, this latter mechanism is not an artifact of surface immobilization, since the rate constants of *T11O* dissociation from origami in solution and on a microscope slide are similar (Supporting Figure S9).

To further test the proposed spacing-dependent walking mechanism of *T7+10*, we measured the rate constant of *T7+10* dissociation from origami with 5-nm probe spacing but prepared with a 1:15 mixture of probe oligonucleotide *P* and an inert control oligonucleotide *P**. The control oligonucleotide *P** binds to probe sites on the origami and will dilute out *P* but possesses a scrambled *T7+10* binding sequence that is not complementary to *T7+10*. The *T7+10* strand was observed to dissociate about 3-fold more rapidly from the mixed *P* + *P**

dx.doi.org/10.1021/nl400976s | *Nano Lett.* 2013, 13, 2754−2759

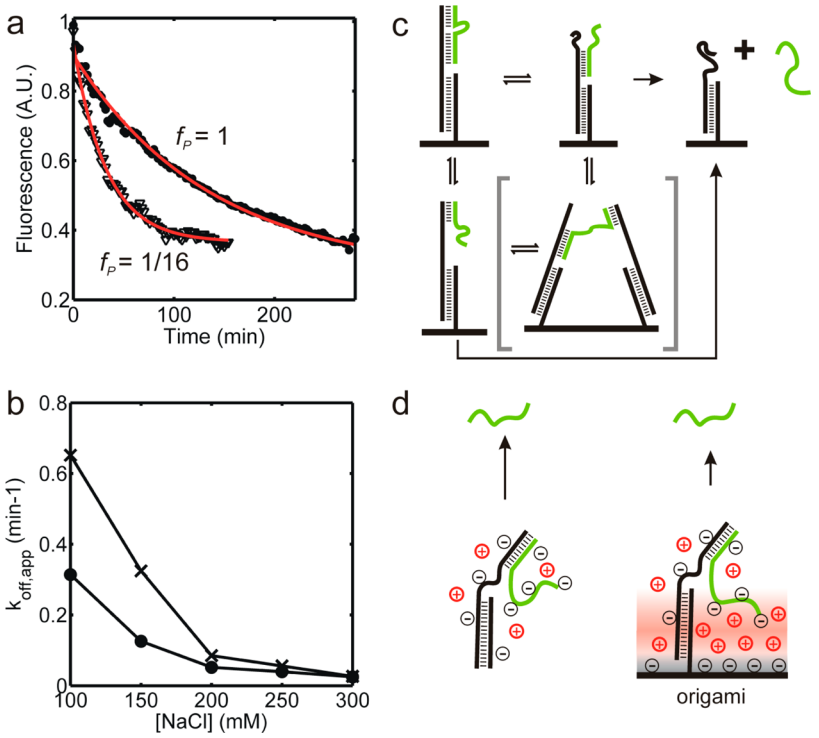

Figure 4. (a) Decay of AF647 signal upon dissociation of *T7+10* from DNA origami with sites spaced by 5 nm bearing only *P* (f_P = 1, ●) or a 1:15 mixture of *P* and the control strand *P** (f_P = 1/16, ▽). The trajectories are fit with a single-exponential decay function of the form $y = Ae^{-kt} + c$ (red curves), yielding apparent rate constants of 0.0074 and 0.030 min^{-1} for f_T = 1 and f_T = 1/16, respectively. (b) Apparent rate constants of *T11O* dissociation from *P* in free solution (×) or bound to origami with a 22 nm spacing between probes (●) in varying concentrations of NaCl. (c) Proposed reaction scheme of spacing-dependent *T7+10* (green) dissociation from origami-bound probe. When other substrate molecules are within reach, a *T7+10* target may walk between them (in brackets), slowing its overall rate of dissociation from the origami tile. (d) Schematic representation of spacing-independent slowing of target (green) dissociation from origami-bound probes (black). In free solution and at relatively low ionic strength (left), electrostatic repulsion between the target and probe is incompletely screened by diffusely bound counterions. In contrast, the negatively charged origami surface (right) recruits a higher local concentration of cations that more effectively screens the negative charge and slows target dissociation.

array (0.03 min^{-1}) than the original *P*-only array (0.009 min^{-1}, Figure 4a), showing that the spacing-dependent slowing of *T7+10* dissociation depends on the proximity of probes complementary to the target rather than generic oligonucleotides. This finding rules out steric crowding as the cause of spacing-dependent dissociation kinetics and strongly suggests a mechanism of walking or hopping for the *T7+10* molecule, in which dissociation from the origami tile is slowed by the ability of *T7+10* molecules to bridge or hop between adjacent probe molecules by using their two binding arms for bipedal walks (Figure 4c). This type of bridging has been hypothesized before as a possible explanation for complex hybridization behavior of targets having a central mismatch with a probe in DNA microarrays of similar density as our nanopegboards, which can slow down the approach to equilibrium or thermodynamically compensate for the mismatch.[29] Consistent with these observations, our findings suggest that such bridging behavior reduces thermodynamic selectivity by slowing dissociation of partially mismatched targets. In contrast, *T11* and *T11O* can each form only a single helical stem with the probe, and this helix must melt before either of these targets can form new base pairing interactions with another probe, precluding any bridging or walking between substrates.

To further test the second, spacing-independent mechanism by which dissociation of both *T7+10* and *T11O* from the origami surface is slowed, we measured the apparent rate constant of *T11O* dissociation in the presence of varying concentrations of NaCl. We hypothesized that the perturbation of kinetics by an origami tile is based on changes in the electrostatic environment so that we expected the extent of this perturbation to depend on ionic strength, as a higher (local) concentration of cations should more effectively shield the electrostatic repulsion between negatively charged phosphate groups in the probe and target DNA strands. We found that the difference between the rate constants of target dissociation from probes on origami and in free solution is greatest at low salt (100−150 mM NaCl), becoming similar or identical at 250−300 mM NaCl (Figure 4b). This observation suggests that, surprisingly, in low salt conditions the negative charges of phosphate groups are screened more effectively at the surface of an origami tile than in free solution. We therefore propose that the presence of a large DNA tile aids in charge screening by enriching the immediate environment in positive counterions, especially at low ionic strength (Figure 4d). The higher local concentration of cations at the origami surface actively promotes sandwich-like interactions between the negatively charged targets and origami surface via an intervening, diffuse layer of metal cations. Such electrostatic screening or sandwiching would have a larger influence on longer strands such as *T7+10* and *T11O* (with more negative charges) than shorter ones such as *T11*. We note that this interpretation is compatible with a prior report in which the dissociation kinetics of a short 9-nucleotide DNA oligomer were not significantly perturbed at the surface of an origami tile.[19]

dx.doi.org/10.1021/nl400976s | *Nano Lett.* 2013, 13, 2754−2759

In summary, we have shown that the patterning of binding probes on individual DNA origami nanopegboards can have a significant effect on the apparent kinetics and, by extension, thermodynamics of target binding to the probes. The magnitude of these deviations depends on the size and mode of binding of oligonucleotide targets, the density of probes on the tile, and ionic conditions. For short DNA strands such as the 11-mer *T11*, the presence of a DNA tile has minimal impact on hybridization kinetics, consistent with the findings of previous studies.[19,20] However, for larger molecules such as *T7+10* and *T11O*, more complex modes of binding and electrostatic interactions can have a pronounced effect, particularly on the dissociation rate constant. As quantitatively predictable performance becomes more important for DNA nanodevices, such as those coordinated by molecular computing circuits, it will be increasingly important to understand the influences of DNA nanostructures on the chemical reactions they organize.

■ ASSOCIATED CONTENT

Supporting Information

Materials and methods; Figures S1−S9. This material is available free of charge via the Internet at http://pubs.acs.org.

■ AUTHOR INFORMATION

Corresponding Author

*E-mail: nwalter@umich.edu.

Notes

The authors declare no competing financial interest.

■ ACKNOWLEDGMENTS

This work was partially funded by the National Science Foundation (NSF) Collaborative Research award EMT/MISC CCF-0829579 and the Department of Defense MURI award W911NF-12-1-0420. A.J.B. acknowledges support from a Rackham Predoctoral Fellowship.

■ REFERENCES

(1) He, Y.; Liu, D. R. *Nat. Nanotechnol.* **2010**, *5*, 778−782.
(2) Gu, H.; Chao, J.; Xiao, S.-J.; Seeman, N. C. *Nature* **2010**, *465*, 202−205.
(3) Lund, K.; Manzo, A. J.; Dabby, N.; Michelotti, N.; Johnson-Buck, A.; Nangreave, J.; Taylor, S.; Pei, R.; Stojanovic, M. N.; Walter, N. G.; Winfree, E.; Yan, H. *Nature* **2010**, *465*, 206−210.
(4) Stein, I. H.; Schüller, V.; Böhm, P.; Tinnefeld, P.; Liedl, T. *ChemPhysChem* **2011**, *12*, 689−695.
(5) Fu, J.; Liu, M.; Liu, Y.; Woodbury, N. W.; Yan, H. *J. Am. Chem. Soc.* **2012**, *134*, 5516−5519.
(6) Douglas, S. M.; Bachelet, I.; Church, G. M. *Science* **2012**, *335*, 831−834.
(7) Andersen, E. S.; Dong, M.; Nielsen, M. M.; Jahn, K.; Subramani, R.; Mamdouh, W.; Golas, M. M.; Sander, B.; Stark, H.; Oliveira, C. L. P.; Pedersen, J. S.; Birkedal, V.; Besenbacher, F.; Gothelf, K. V.; Kjems, J. *Nature* **2009**, *459*, 73−76.
(8) Lo, P. K.; Karam, P.; Aldaye, F. A.; McLaughlin, C. K.; Hamblin, G. D.; Cosa, G.; Sleiman, H. F. *Nat. Chem.* **2010**, *2*, 319−328.
(9) Han, D.; Pal, S.; Liu, Y.; Yan, H. *Nat. Nanotechnol.* **2010**, *5*, 712−717.
(10) Qian, L.; Winfree, E. *Science* **2011**, *332*, 1196−1201.
(11) Alon, U. *An Introduction to Systems Biology: Design Principles of Biological Circuits*, 1st ed.; Chapman and Hall/CRC: New York, 2006.
(12) Michelotti, N.; Johnson-Buck, A.; Manzo, A. J.; Walter, N. G. *Wiley Interdiscip. Rev.: Nanomed. Nanobiotechnol.* **2012**, *4*, 139−152.
(13) Wilkins Stevens, P.; Henry, M. R.; Kelso, D. M. *Nucleic Acids Res.* **1999**, *27*, 1719−1727.
(14) Watterson, J. H.; Piunno, P. A. E.; Wust, C. C.; Krull, U. J. *Langmuir* **2000**, *16*, 4984−4992.
(15) Herne, T. M.; Tarlov, M. J. *J. Am. Chem. Soc.* **1997**, *119*, 8916−8920.
(16) Steel, A. B.; Herne, T. M.; Tarlov, M. J. *Anal. Chem.* **1998**, *70*, 4670−4677.
(17) Peterson, A. W.; Heaton, R. J.; Georgiadis, R. M. *Nucleic Acids Res.* **2001**, *29*, 5163−5168.
(18) Mirmomtaz, E.; Castronovo, M.; Grunwald, C.; Bano, F.; Scaini, D.; Ensafi, A. A.; Scoles, G.; Casalis, L. *Nano Lett.* **2008**, *8*, 4134−4139.
(19) Jungmann, R.; Steinhauer, C.; Scheible, M.; Kuzyk, A.; Tinnefeld, P.; Simmel, F. C. *Nano Lett.* **2010**, *10*, 4756−4761.
(20) Pinheiro, A. V.; Nangreave, J.; Jiang, S.; Yan, H.; Liu, Y. *ACS Nano* **2012**, *6*, 5521−5530.
(21) Douglas, S. M.; Dietz, H.; Liedl, T.; Hogberg, B.; Graf, F.; Shih, W. M. *Nature* **2009**, *459*, 414−418.
(22) Johnson-Buck, A. E.; McDowell, S. E.; Walter, N. G. *Met. Ions Life Sci.* **2011**, *9*, 175−196.
(23) Rueda, D.; Wick, K.; McDowell, S. E.; Walter, N. G. *Biochemistry* **2003**, *42*, 9924−9936.
(24) Duckett, D. R.; Murchie, A. I.; Lilley, D. M. *EMBO J.* **1990**, *9*, 583−590.
(25) Langecker, M.; Arnaut, V.; Martin, T. G.; List, J.; Renner, S.; Mayer, M.; Dietz, H.; Simmel, F. C. *Science* **2012**, *338*, 932−936.
(26) Johnson-Buck, A.; Nangreave, J.; Kim, D.-N.; Bathe, M.; Yan, H.; Walter, N. G. *Nano Lett.* **2013**, *13*, 728−733.
(27) Morrison, L. E.; Stols, L. M. *Biochemistry* **1993**, *32*, 3095−3104.
(28) Moreira, B. G.; You, Y.; Behlke, M. A.; Owczarzy, R. *Biochem. Biophys. Res. Commun.* **2005**, *327*, 473−484.
(29) Levicky, R.; Horgan, A. *Trends Biotechnol.* **2005**, *23*, 143−149.
(30) Kim, J.; Winfree, E. *Mol. Syst. Biol.* **2011**, *7*, 465.
(31) Stojanovic, M. N.; Stefanovic, D. *J. Comput. Theor. Nanosci.* **2011**, *8*, 434−440.
(32) Stojanovic, M.; Stefanovic, D. *Nat. Biotechnol.* **2003**, *21*, 1069−1074.